Neuron
Article

Modeling the Spatial Reach of the LFP

Henrik Lindén,[1,2] Tom Tetzlaff,[1,3] Tobias C. Potjans,[3,4,5] Klas H. Pettersen,[1,6] Sonja Grün,[3,7,8] Markus Diesmann,[3,4,8,9] and Gaute T. Einevoll[1,6,*]
[1]Department of Mathematical Sciences and Technology, Norwegian University of Life Sciences, N-1432 Ås, Norway
[2]Department of Computational Biology, School of Computer Science and Communication, Royal Institute of Technology (KTH), 10044 Stockholm, Sweden
[3]Institute of Neuroscience and Medicine (INM-6), Computational and Systems Neuroscience, Research Center Jülich, 52425 Jülich, Germany
[4]Brain and Neural Systems Team, RIKEN Computational Science Research Program, Wako, Saitama 351-0198 Japan
[5]Faculty of Biology III, Albert-Ludwigs-University Freiburg, 79104 Freiburg, Germany
[6]Centre for Integrative Genetics (CIGENE), Norwegian University of Life Sciences, N-1432 Ås, Norway
[7]Theoretical Systems Neurobiology RTWH Aachen University, 52062 Aachen, Germany
[8]RIKEN Brain Science Institute, Wako, Saitama 351-0198, Japan
[9]Medical Faculty, RTWH Aachen University, 52074 Aachen, Germany
*Correspondence: gaute.einevoll@umb.no
DOI 10.1016/j.neuron.2011.11.006

SUMMARY

The local field potential (LFP) reflects activity of many neurons in the vicinity of the recording electrode and is therefore useful for studying local network dynamics. Much of the nature of the LFP is, however, still unknown. There are, for instance, contradicting reports on the spatial extent of the region generating the LFP. Here, we use a detailed biophysical modeling approach to investigate the size of the contributing region by simulating the LFP from a large number of neurons around the electrode. We find that the size of the generating region depends on the neuron morphology, the synapse distribution, and the correlation in synaptic activity. For uncorrelated activity, the LFP represents cells in a small region (within a radius of a few hundred micrometers). If the LFP contributions from different cells are correlated, the size of the generating region is determined by the spatial extent of the correlated activity.

INTRODUCTION

The local field potential (LFP) usually refers to the low-frequency part ($\lesssim$ 500 Hz) of an extracellular voltage signal recorded inside the brain. It is among the oldest experimental measures of neural activity and has been widely used to investigate network mechanisms involved in sensory processing (Mitzdorf, 1985; Di et al., 1990; Kandel and Buzsáki, 1997; Schroeder et al., 1998; Henrie and Shapley, 2005; Belitski et al., 2008; Montemurro et al., 2008; Szymanski et al., 2009), motor planning (Scherberger et al., 2005; Roux et al., 2006), and higher cognitive processes including attention, memory, and perception (Pesaran et al., 2002; Kreiman et al., 2006; Liu and Newsome, 2006; Womelsdorf et al., 2006; Montgomery and Buzsáki, 2007; Colgin et al., 2009). In combination with multiunit activity (MUA), the high-frequency ($\gtrsim$ 500 Hz) part of the extracellular voltage, it has been found useful for inferring key properties of network dynamics (Denker et al., 2010, 2011; Kelly et al., 2010) and population-specific laminar activity (Einevoll et al., 2007). In addition, the LFP has been suggested as a candidate signal for steering motor prosthetic devices (Mehring et al., 2003; Andersen et al., 2004; Rickert et al., 2005) as it is relatively easy to record and more stable than single-unit activity.

Despite its wide use, there is still limited knowledge about the relation between the LFP and the underlying neural activity. The LFP is believed to primarily reflect synaptic activity in a neural ensemble in the vicinity of the recording electrode (Mitzdorf, 1985; Nunez, 2006) and to represent a weighted sum of all transmembrane currents following synaptic activation. The details of the extracellular field generated by a single synaptic current depend on the cell morphology as well as the spatial positions of the synapse and recording electrode (Lindén et al., 2010). The LFP most likely reflects the activity of several populations of different cell types, but due to their so-called "open-field" arrangement dendritic synapses on pyramidal cells have been hypothesized to be a major contributor to the LFP signal (Lorente de No, 1947; Rall, 1962; Mitzdorf, 1985; Johnston and Wu, 1995). The interpretation of the LFP is further complicated by the fact that, in contrast to the MUA which represents the spiking output of a local population, the LFP reflects input to the population which might originate both from local recurrent connections as well as other more distant brain regions.

The duration of spikes, the extracellular signatures of neuronal action potentials, is so short that a recorded MUA often can be sorted into nonoverlapping contributions from individual neurons surrounding the electrode contact (Buzsáki, 2004). In this context, one may thus ask: how many neurons can an electrode record from? Since the individual neuronal contributions to the LFP are largely overlapping in time, this question is not suitable in the context of LFP. Instead, one may ask how large the cortical region is that generates the LFP. Several recent

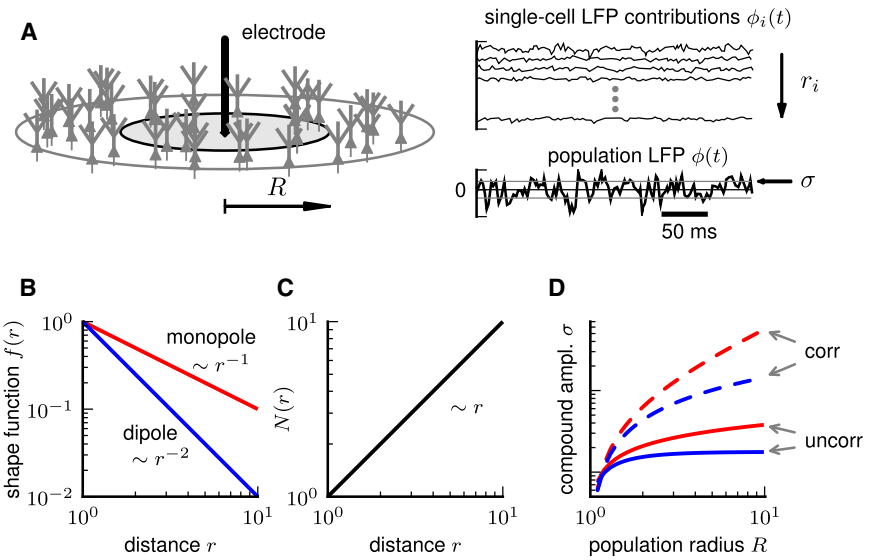

Figure 1. Generation of Population LFP

(A) Sketch of the model setup. Cells are homogeneously distributed on a disc of radius R with the tip of the electrode in the center. The sum of LFP contributions $\phi_i(t)$ of individual cells at distances r_i results in a population LFP $\phi(t)$. The dependence of its amplitude $\sigma(R)$ on the population radius R (see panel D) defines the electrode reach (see text).

(B) Illustration of dependence of the single-cell LFP amplitude $f(r)$ (shape function) on cell-electrode distance r for hypothetical current monopole (red) and current dipole sources (blue).

(C) Illustration of number $N(r)$ of cells on a ring of radius r.

(D) Illustration of dependence of compound amplitude $\sigma(R)$ on population radius R for populations of uncorrelated ($c_\phi = 0$; solid curves) and correlated ($c_\phi = 1$; dashed curves) monopole (red) and dipole sources (blue).

experimental studies have addressed this question (Kreiman et al., 2006; Liu and Newsome, 2006; Berens et al., 2008a; Katzner et al., 2009; Xing et al., 2009) but have reported different results ranging from a few hundred micrometers (Katzner et al., 2009; Xing et al., 2009) to several millimeters (Kreiman et al., 2006). How can the results be so different? One possibility is that the LFP reported in various experiments stems from different types of neuronal populations or that the electrodes have been placed differently. Moreover, different stimulation paradigms have been used, likely resulting in different levels of correlations between the synaptic currents providing the recorded LFP. It has long been suggested that the LFP is dominated by synchronously driven dendritic input on pyramidal cells (Mitzdorf, 1985), but it has until now been unclear how the amount and spatial extent of correlations in synaptic activity influence the LFP.

In the present study, we investigate various key factors determining the size of the region an LFP electrode can "see," in particular, the neuronal morphology, synaptic distribution, level of correlation in synaptic activity, and the position of the recording electrode. We use a biophysical forward-modeling approach to address these questions (Holt and Koch, 1999; Pettersen et al., 2008; Pettersen and Einevoll, 2008; Lindén et al., 2010) and simulate the LFP signal from synaptically activated populations of morphologically reconstructed cortical cells. The LFP amplitude generally increases with increasing radius of the model population, but typically it flattens out beyond a certain radius, here termed the *spatial reach*. For uncorrelated synaptic activity, we find this spatial reach to be only a few hundred micrometers, implying that the recorded LFP is generated by a small population of neurons surrounding the electrode. This result is in line with findings in recent experimental studies (Katzner et al., 2009; Xing et al., 2009). However, for particular synaptic distributions onto pyramidal cells, we find the reach of the LFP to be much larger and depend strongly on the level and spatial scale of correlations in the synaptic input, putatively explaining the disparate results reported in other experimental studies (Kreiman et al., 2006; Liu and Newsome, 2006; Berens et al., 2008a; Katzner et al., 2009; Xing et al., 2009). Our simulation findings are supported by analytical results using a simplified, yet as it turned out, accurate model of LFP generation. This model encapsulates the dependence of the population LFP on the spatial decay of single-neuron LFP contributions and correlation of synaptic input.

RESULTS

The spatial reach of the local field potential is investigated by studying how the amplitude σ of a measured compound potential $\phi(t)$ depends on the size of cylindrical populations of synaptically activated neurons surrounding the electrode (see Experimental Procedures and Figure 1A). We define the LFP amplitude σ as the standard deviation of the compound LFP signal $\phi(t)$ across time. With increasing population radius R, more and more cells contribute to the compound signal $\phi(t)$. The amplitude $\sigma(R)$ is thus expected to increase with R. On the other hand, the contribution to the potential from a single neuron decreases with its distance r from the electrode (Lindén et al., 2010). Intuitively, one might therefore expect that $\sigma(R)$ approaches a constant value σ^* as the population size R increases. If so, it is natural to define the *reach* R^* of the electrode as the population size at which the signal amplitude captures a certain fraction α of this limit value σ^*. In the present article, we set α to 95 %. It is, however, a priori not clear that $\sigma(R)$ converges, i.e., that a finite limit value σ^* and thus a finite reach R^* indeed exist. Below we will therefore first consider a simplified model to demonstrate which factors shape the dependence of the LFP amplitude $\sigma(R)$ on the population size R and to illustrate under which conditions the spatial reach is finite. Next, we investigate these factors in detail by means of comprehensive numerical simulations of the LFP generated by cortical populations consisting of thousands of neurons with realistic dendritic morphologies.

Table 1

	$c_\phi = 0$	$c_\phi \neq 0$
$\gamma \leq 1$	diverging	diverging
$1 < \gamma \leq 2$	converging	diverging
$\gamma > 2$	converging	converging

Convergence behavior of the compound amplitude $\lim_{R\to\infty}\sigma(R)$ for a power-law shape function $f(r) \sim 1/r^\gamma$ showing dependence on decay exponent γ and correlation c_ϕ.

Existence of a Finite Spatial Reach of LFP

This idea suggests that the amplitude σ generated by a population of neuronal sources surrounding the electrode is essentially controlled by three factors:

- The attenuation $f(r)$ of the contribution to the LFP signal from a single neuron with increasing distance r (Figure 1B),
- The number density $N(r)$ of neuronal sources positioned on a ring of radius r around the electrode (Figure 1C), and
- The correlation c_ϕ between the signals generated by the individual neuronal sources.

The distance-dependent attenuation $f(r)$ of the extracellular potential around a neuron is determined by the distribution of the underlying transmembrane current density (Pettersen and Einevoll, 2008; Lindén et al., 2010). The potential generated by a pure current dipole source, for example, typically decreases in amplitude as $1/r^2$ with distance r (blue curve in Figure 1B). A hypothetical point source, in contrast, would generate a potential which decays in amplitude as $1/r$ (red curve in Figure 1B).

Assuming a constant area density of neuronal sources, the decrease in amplitude is to some extent compensated by the increase in the number of neurons with increasing distance from the electrode. In this article, we consider populations of neurons symmetrically distributed around the electrode on a 2D plane with a constant density ρ. The number $N(r)\Delta r = 2\pi r\rho\Delta r$ of neurons on a narrow ring of radius r and width Δr will then grow linearly with the population radius (Figure 1C).

If the single-cell contributions to the LFP are uncorrelated, the variances of the signals generated by the individual cells positioned on a narrow ring of radius r will sum up, so that the amplitude σ of the compound signal will be proportional to $\sqrt{N(r)}f(r)$. This number decreases with distance both for monopole ($\sqrt{N(r)}f(r) \sim 1/r^{1/2}$) and dipole sources ($\sqrt{N(r)}f(r) \sim 1/r^{3/2}$). For a population of dipoles, integration of all rings up to a radius R results in a compound amplitude $\sigma(R)$ which converges with increasing population size R toward a constant value σ^* (solid blue curve in Figure 1D). For a population of monopoles, however, $\sigma(R)$ will grow unbounded (solid red curve in Figure 1D). If the single-cell contributions to the LFP potential are perfectly correlated, on the other hand, the total variance σ_r^2 for neurons on a ring of radius r will be proportional to $[N(r)f(r)]^2$ (see Experimental Procedures). In this case, both the monopole and the dipole population exhibit diverging compound amplitudes $\sigma(R)$ with increasing population radius (dashed curves in Figure 1D).

In Experimental Procedures, we derive a simplified model to describe $\sigma(R)$ and its dependence on the shape of $f(r)$ and the correlation c_ϕ between single-neuron LFP contributions. In this framework, the potential $\phi_i(t) = \xi_i(t)f(r_i)$ generated by a single neuron i is assumed to factorize into a purely time-dependent part $\xi_i(t)$ and a purely distance-dependent part $f(r_i)$. Here, $\xi_i(t)$ reflects the temporal structure of the total synaptic input onto the neuronal sources, while the shape function $f(r_i)$ describes the amplitude of the LFP signal as a function of the cell position. This latter function is determined by the electrical and morphological properties of the neuron, as well as its position and orientation with respect to the electrode contact. The distance r_i denotes the radial distance of the cell from the electrode. The compound LFP amplitude $\sigma(R)$ from a homogeneous population of neurons around the electrode tip reads (cf. Experimental Procedures and Equation 6)

$$\sigma(R) = \sigma_\xi \sqrt{(1 - c_\phi)g_0(R) + c_\phi g_1(R)}. \quad (1)$$

Here σ_ξ is the amplitude (standard deviation) of the synaptic input current, and the two functions

$$g_0(R) = \int_0^R dr\, N(r)f(r)^2 \text{ and } g_1(R) = \left(\int_0^R dr\, N(r)f(r)\right)^2 \quad (2)$$

describe the competition between $f(r)$ and $N(r) = 2\pi r\rho$ for the uncorrelated and correlated case, respectively (see Equation 7). To further demonstrate that the convergence of $\sigma(R)$ essentially is determined by $f(r)$ and the correlation c_ϕ, we summarize in Table 1 the results for when the shape function follows a power-law, $f(r) \sim 1/r^\gamma$, (see Experimental Procedures and Equation 9). In the presence of spatially homogeneous correlations, we observe that $\sigma(R)$ approaches a finite value for increasing R only for decay exponents $\gamma > 2$.

Distance Dependence of Single-Cell LFP Contributions

To determine $f(r)$, i.e., how the amplitude of the single-cell LFP contribution decays with the cell's distance from the electrode, we placed reconstructed morphologies of layer 3 (L3) pyramidal, layer 4 (L4) stellate, and layer 5 (L5) pyramidal cells (Mainen and Sejnowski, 1996; Figure 2A) at different radial distances r from a set of recording positions (one in each cortical layer) and computed at each distance the mean LFP amplitude from 100 cells receiving synaptic input (see Experimental Procedures). To mimic a scenario with laminar cortical populations, all cells of a particular cell type were placed at the same cortical depth (according to cortical layer), but each cell's morphology was randomly rotated along its vertical axis to introduce heterogeneity in the population. In order to investigate the effect of the spatial distribution of synaptic inputs, we placed synapses either homogeneously over the whole dendritic structure or only apically or basally (Figure 2A; see Experimental Procedures). Each neuron received 1,000 uncorrelated Poissonian spike trains with an individual firing rate of 5 spikes/s.

For all combinations of cell type and recording position, the amplitude of the LFP contribution from a neuron placed sufficiently far away from the electrode decays as $\sim 1/r^2$ with radial electrode distance r, with a less steep decay at the center of

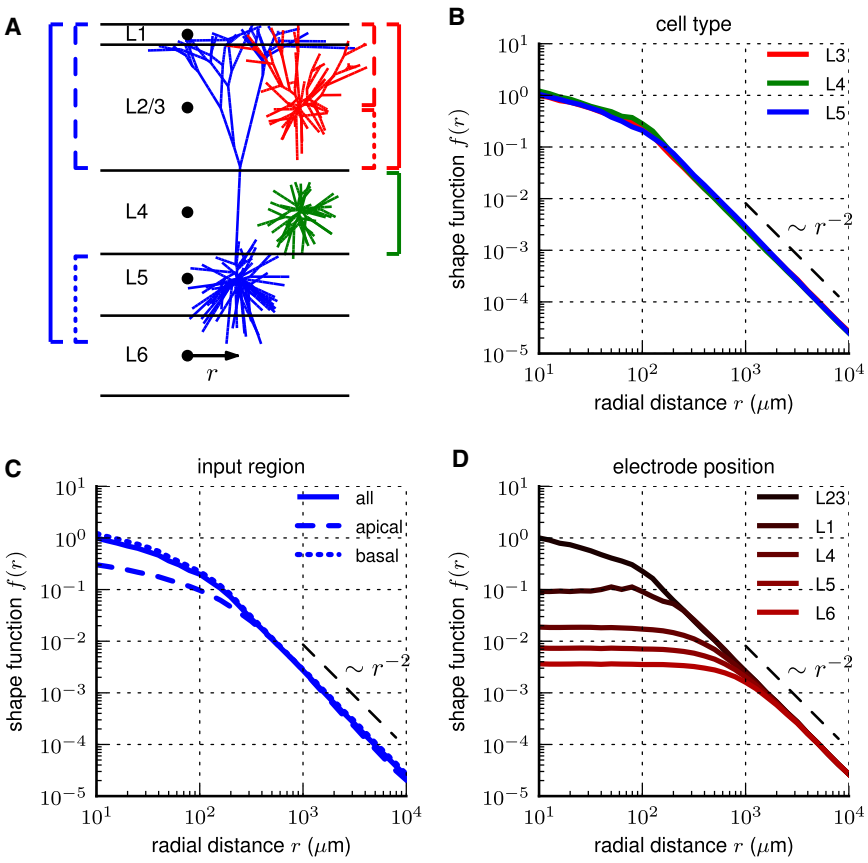

Figure 2. Distance Dependence of Amplitude of Single-Neuron LFP Contributions

(A) Illustration of reconstructed cell morphologies used in simulations, L3 pyramidal cell (red), L4 stellate cell (green), L5 pyramidal cell (blue), positioned at their assumed population depth. Electrode positions are shown as black dots. The neurons were placed at different radial positions r, and the shape function $f(r)$ describing the amplitude of single cell LFP contributions was calculated for cells receiving either homogenous (solid brackets), apical (dashed brackets), or basal (dotted bracket) synaptic input.

(B) LFP amplitude for the three different cell types, recorded in the soma layer for each cell type, normalized to the value for the L3 cell at distance $r = 10$ μm.

(C) LFP amplitude for L5 cell recorded in the L5 soma layer for different synapse distributions, normalized against the value for homogeneous synaptic input (at $r = 10$ μm).

(D) LFP amplitude at different recording depths for L3 cell receiving homogenous inputs, normalized against the value at $r = 10$ μm for electrode placement in L2/3. In (B)–(D) thin dashed lines indicate decay proportional to r^{-2}.

the population (Figures 2B–2D). The distance where the transition to $1/r^2$-decay occurred varied with recording depth (Figure 2D) as well as with the distribution of synapses over the dendrites (Figure 2C). The differences in this "transition distance" between the L3, L4, and L5 neurons are, however, small for the LFPs recorded in the respective soma layers (Figure 2B). The large variation of the LFP with recording position, illustrated for the L3 cell in Figure 2D, can largely be attributed to the geometrical effect that even for small radial distances, the distance between the neuron and the depth-shifted electrode may be sizable. As we will see, this has important consequences for the LFP reach when recording from a laminar position above or below the soma layer of the active cortical population.

Dependence of LFP Reach on Cell Morphology, Synapse Distribution, and Electrode Depth

We next investigated how the spatial reach of the compound population LFP depends on neuronal morphologies and spatial synapse distribution. To this end, we simulated laminar populations consisting of 10,000 reconstructed cells placed in a cylindrical volume with a 1 mm radius (Figure 1A; see Experimental Procedures). All cells in a population were positioned at the same cortical depth, corresponding to the depth depicted for single neurons in Figure 2A (see Experimental Procedures), but each cell was randomly rotated around its vertical axis. We first used uncorrelated spike trains as input and computed the amplitude $\sigma(R)$ of the LFP generated by cells positioned within a population radius R centered around a vertical recording electrode. Increasing the radius of the population quickly increased the LFP amplitude up to a constant value that did not change when the population radius was further increased (Figure 3A). We defined the 'spatial reach' of the LFP as the population radius where the LFP amplitude had reached 95 % of the maximum value found in our simulations, i.e., for $R = R_{max}$ = 1,000 μm (Figure 3A2). For the case with synapses homogeneously distributed over the dendrites, plotting of the LFP reach as a function of depth position of the electrode revealed that the reach was always smallest in the soma layer of the activated population (Figure 3C). For all three neuronal populations, 95% of the amplitude of the signal recorded in the soma layer came from neurons within a radius smaller than 200 μm (Figure 3D). By plotting the LFP amplitude as a function of cortical depth, we further found the largest LFP amplitudes at the soma level (Figure 3E). We therefore conclude that when the synaptic activity is uncorrelated, the LFP is rather local, both in terms of horizontal reach and amplitude variation in the vertical direction.

Changing the synaptic distributions to either only apical or only basal dendrites for the pyramidal cells gave a different depth dependence for both the reach and the amplitude of the LFP for the L5 population, whereas the results for the L3 population were largely unaffected (Figures 3D and 3E). For the apically activated L5 population both the LFP amplitude and the spatial reach are similar for the electrode contacts positioned in L2/3 and the L5 soma layer (Figures 3D3–3E3). This demonstrates that these qualitative features of the LFP are determined both

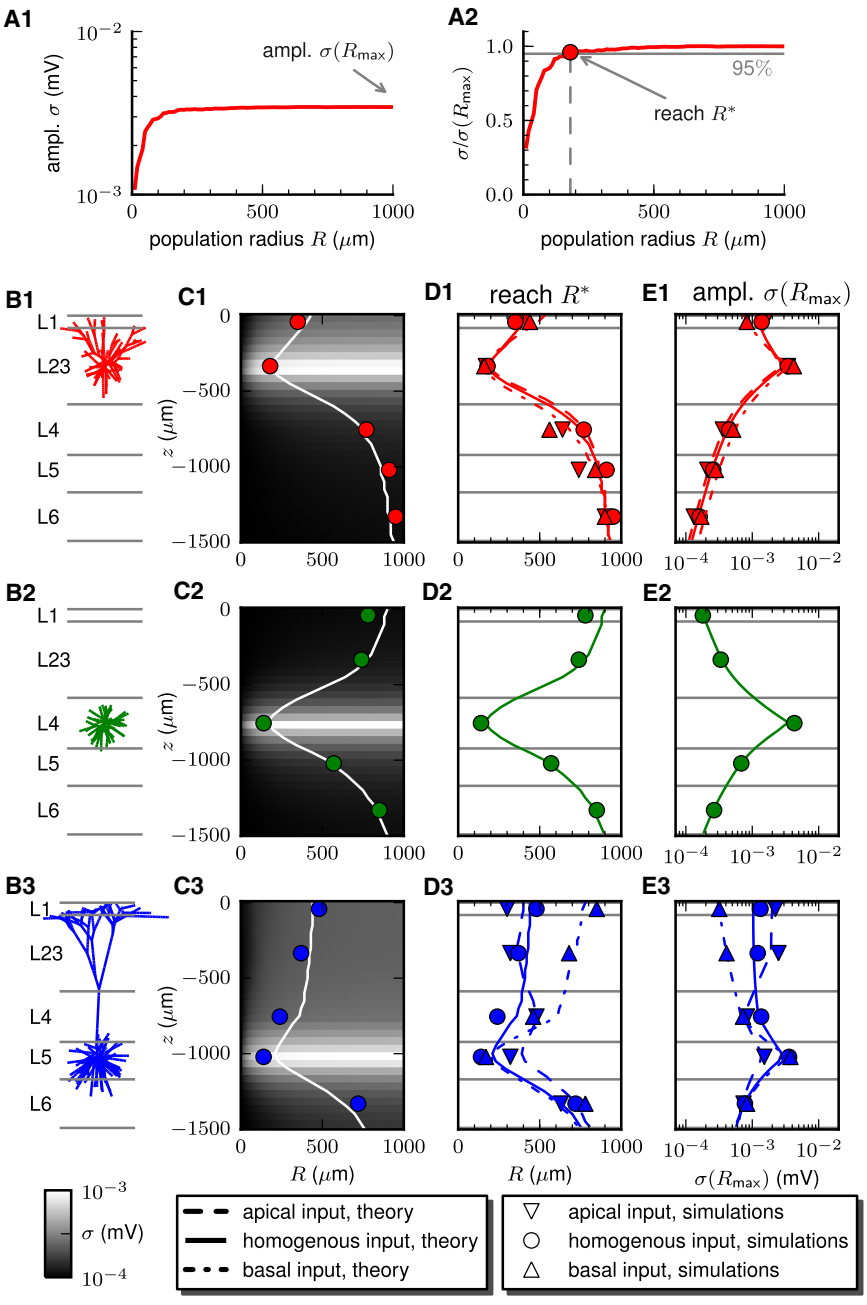

Figure 3. Depth Dependence of Population LFP for Uncorrelated Synaptic Activity

(A1) LFP amplitude σ as a function of population radius R for a population of L3 cells receiving uncorrelated input. LFP was recorded at the soma level of L2/3. (A2) Normalized LFP amplitudes for situation in (A1). LFP reach R^* is defined as the radius for which the LFP amplitude reaches 95 % of the value for R_{max} = 1,000 μm.

(B) Cell morphologies and their vertical placement according to cortical layers.

(C) LFP amplitude σ (gray scale: predictions from simplified model) and LFP reach (circles: simulations, white lines: simplified model) for uncorrelated homogenous synaptic input as a function of electrode depth z.

(D) LFP reach R^* for different synaptic distributions.

(E) LFP amplitude $\sigma(R_{max})$ for different synaptic distributions (symbols: simulation results, lines: simplified model).

by the spatial distributions of the synaptic inputs and the neuronal morphology, in particular the depth profile of the total dendritic area (Lindén et al., 2010).

We next compared the numerical simulations with predictions of the simplified model: by using the detailed single-cell decay functions $f(r)$ obtained above (Figure 2), we numerically integrated the simplified model (Equation 1). As seen in Figure 3, the predictions of the simplified model agree excellently with the results of the comprehensive numerical simulations, suggesting that our simplified model indeed captures the salient features of LFP generation from neuronal populations.

Dependence on Correlations in Synaptic Activity

How do these results change when the synaptic inputs to different cells in the population are correlated? We used the same simulation setup as above with the difference that spike trains to different cells were drawn from a finite pool of presynaptic spike trains (Figure 4A). This induced a mean correlation c_ξ between the synaptic input currents to different cells due to common input. By varying the size of the pool of presynaptic spike trains n_{pool} we could vary the input correlation c_ξ (see Experimental Procedures).

As predicted by the simplified model (Equation 1), inducing correlations between single cell LFP contributions changed the total LFP amplitude in three respects: (1) the LFP amplitude σ becomes considerably higher (Figures 4C1–4C3 and 4F1), (2) the reach R^* of the LFP (as before defined as the population radius where the amplitude had reached 95 % of the value for R = 1,000 μm) generally increases (Figures 4D1–4D3 and 4E1), and (3) the LFP amplitude σ no longer appears to converge to a fixed value with increasing population radius. Population simulations for different cell types (L3 pyramidal, L4 stellate, and L5 pyramidal cells) and synaptic distributions (apical, homogeneous or basal) (Figure 4B) revealed that the extent to which correlations had an effect on the total LFP amplitude was highly dependent on cell type and spatial distribution of synapses on the dendritic structure. The effects were largest for the L5 pyramidal cell population whereas the LFP amplitude from L4 stellate cell population was largely unaffected (Figures 4E1 and 4F1). It also depended on the spatial distribution

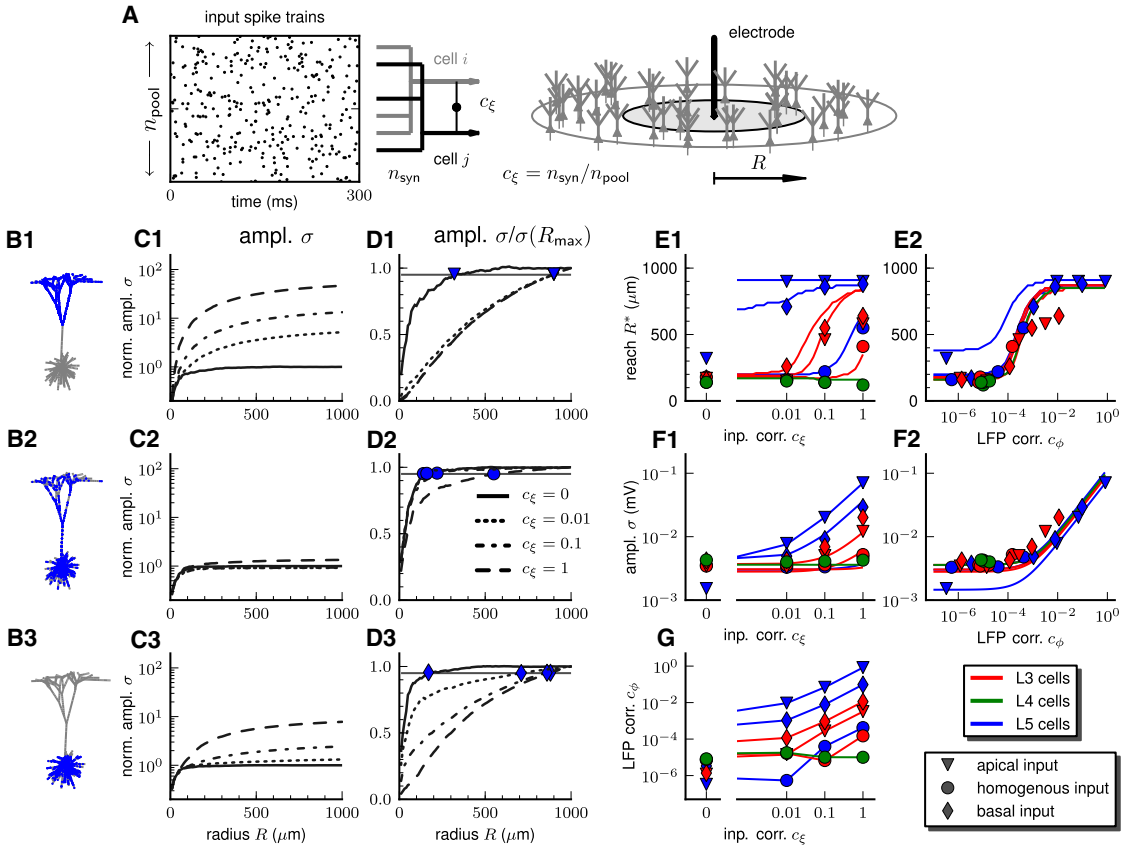

Figure 4. Reach of LFP Depends on Level of Input Correlations

(A) Illustration of simulation setup.

(B–D) LFP amplitude σ as a function of population radius *R* (C) and LFP reach *R** (D) for population of L5 pyramidal cells receiving synaptic input at apical dendrites (B1), homogeneously distributed (B2) or at basal dendrites (B3) for LFP recorded at the soma level of the population. Reach *R** was defined as the radius *R* where the amplitude σ has reached 95% of the value $\sigma(R_{max}$ = 1,000 μm).

(E and F) LFP reach *R** and LFP amplitude $\sigma(R_{max}$ = 1,000) μm) for different cell types and input scenarios, either as a function of input correlation c_ξ (E1 and F1) or resulting mean pairwise correlation between single cell LFP contributions c_ϕ (E2 and F2).

(G) Relation between synaptic input correlation c_ξ and LFP correlation c_ϕ. In (E)–(F) lines represent results from the simplified model using numerically derived shape functions *f*(*r*) and numerical values of correlation transfer (from c_ξ to c_ϕ) and symbols represent simulation results. In (G), the lines are interpolation of the simulation results.

of synapses: there were pronounced effects for either apical or basal input, but only a modest effect for homogeneous synaptic distributions (Figures 4E1 and 4F1).

To explore these differences further we computed the mean pairwise correlation c_ϕ (see Experimental Procedures and Supplemental Equation 18) between single-cell LFP contributions as a function of input correlation c_ξ for the different cell types and input scenarios (Figure 4G). This provided an explanation for why the effect of correlations was found to be so different for the different cell types and synaptic distributions: for example, LFP contributions are more correlated for L5 pyramidal cells than the other cell types, and apical input gives higher correlations than basal or homogenous input. Thus, the extent to which input correlations have an effect on the reach of LFP depends on how reliably input correlations c_ξ are translated to correlations between LFP contributions c_ϕ. Replotting the LFP reach and amplitude as function of the LFP correlations further supported this interpretation as all simulation results then collapsed onto the same curve (Figures 4E2 and 4F2). This clearly demonstrates the importance of the level of correlation between individual LFP contributions in determining both the reach and amplitude of the LFP.

The results depicted in Figure 4 demonstrate the key role played by synaptic correlations in determining the LFP amplitude. From the analytical formulas in Equations 1 and 2, we further see that the contribution from correlated neuronal sources scales differently with the density of sources $(g_1(R) \sim \rho^2)$ than for uncorrelated sources $(g_0(R) \sim \rho)$. Thus the correlated contributions to the LFP will generally dominate the uncorrelated contributions when the correlation coefficient c_ϕ and/or the source density ρ are large. This is illustrated for particular examples in Figure S1, available online.

Spatial Scale of Correlations

Until now, we have implicitly assumed that the synaptic input to different neurons are equally correlated throughout the whole population. How will the results change if the level of correlation

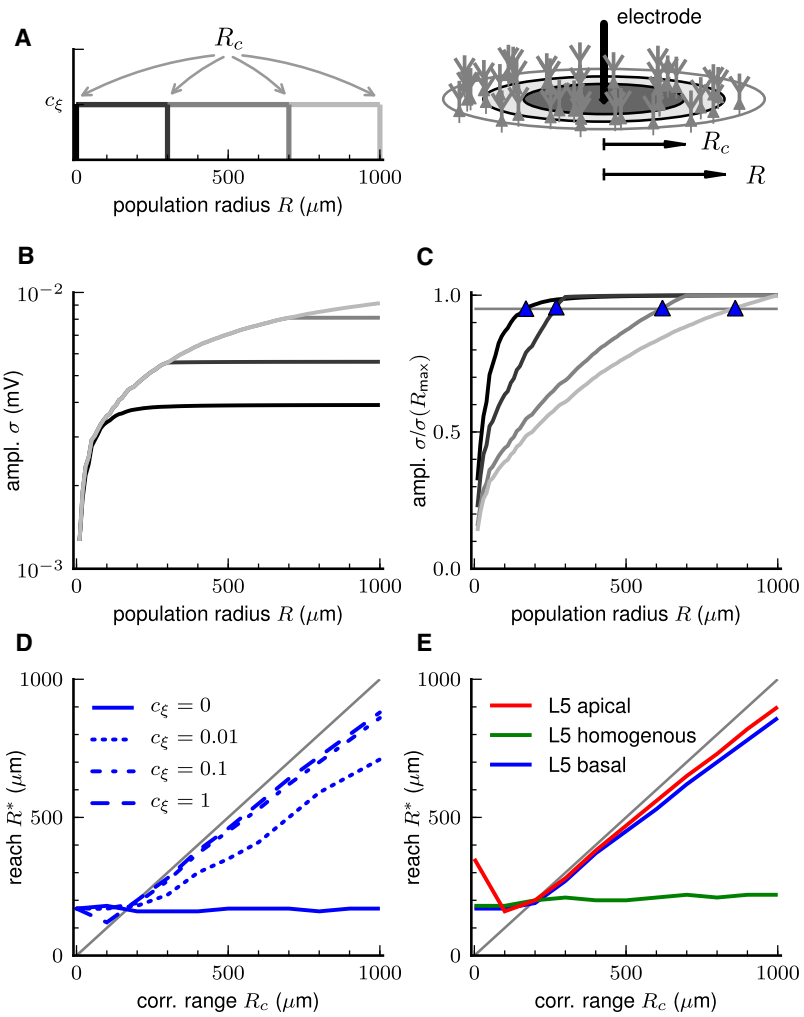

Figure 5. Reach of LFP Depends on Spatial Range of Input Correlations

(A) Illustration of test situation where synaptic inputs to neurons within a radius R_c are uniformly correlated with correlation coefficients c_ξ, while inputs to neurons outside this region are uncorrelated.

(B) LFP amplitude σ for population of L5 cells with synapses distributed on basal dendrites for different values of R_c = [0,300,700,1000] μm (as indicated in A) while total population radius R is 1,000 μm. Input correlation c_ξ is 0.1.

(C) Same as in (B) but normalized to amplitude $\sigma(R_{max}$ = 1,000 μm). Reach R^* is defined as the radius R where the amplitude σ reaches 95% of the maximum value $\sigma(R_{max}$ = 1,000 μm) (blue triangles).

(D) LFP reach for different values of c_ξ for population of L5 cells with basal activation. Note that the deviation from a straight line for the curve for c_ξ = 0 is due to numerical variability in the simulation.

(E) LFP reach for different synaptic distributions when c_ξ = 0.1 In (C) and (D), gray lines correspond to $R^* = R_c$.

between LFP contributions is dependent on the radial distance to the electrode? We studied a simple case where LFP contributions were assumed to be homogeneously correlated only within a certain radius $R_c<R$ (Figure 5A); outside this region the correlation was set to zero. Figure 5B shows the LFP amplitude for a population of basally activated L5 pyramidal neurons for different values of R_c where the input correlation c_ξ in the correlated region was set to 0.1. For the chosen set of example values for R_c, the LFP amplitude increases up to the radius R_c and then quickly converges to a fixed value (Figure 5B). This gives values of the LFP reach close to the values of R_c (Figure 5C). Thus, neurons outside the region of correlated activity contribute minimally to the LFP amplitude. Both the LFP amplitude and the reach are thus largely determined by the spatial scale of the correlated activity. The LFP reach increases in a linear fashion with increasing size R_c of the correlated part of the population, with a slope that depends on the level of input correlation (Figure 5D). Results also vary with the spatial synaptic distribution: as before the observed effects of correlations are large for apical and basal activation, while almost negligible for homogeneous synaptic activation of the L5 population (Figure 5E).

In Vivo-like Input from a Cortical Network Model

The above investigations have focused on generic features of LFP generation, and only the situation with a single type of synaptic input onto neuronal populations has been studied. Cortical populations in vivo receive a variety of inputs, however. These can be either local inputs from the various cell types within the local cortical network or long-range inputs from other brain regions. The synaptic inputs to a single neuron are both excitatory and inhibitory, and different subgroups of synapses may target different dendritic regions. Furthermore, spike trains from different neurons are potentially correlated, providing additional input correlation to that from shared input. To investigate how our generic findings translate to more realistic settings, we embedded the single-cell reconstructions in an in vivo-like environment to test if the range of input correlations c_ξ used so far were realistic, and if the results would pertain in situations where populations received a combination of excitatory, inhibitory and external (long-range) inputs.

We simulated populations of reconstructed cells receiving spike trains generated by a laminar network of integrate-and-fire neurons representing a local cortical microcircuit (Potjans and Diesmann, 2011; Wagatsuma et al., 2011). The network consisted of ~80,000 neurons distributed across four layers, each with one excitatory and one inhibitory population. The choice of neuron numbers in each population was based on anatomical data from cat visual cortex (Binzegger et al., 2004). The size of the network was sufficiently large to incorporate the majority of local synapses impinging on a cortical cell (Braitenberg and Schüz, 1998; Binzegger et al., 2004). Most notably, the data-based connectivity structure of the network (see Supplemental Information) resulted in cell-type-specific firing rates consistent with in vivo data from rat cortex (e.g., de Kock and Sakmann,

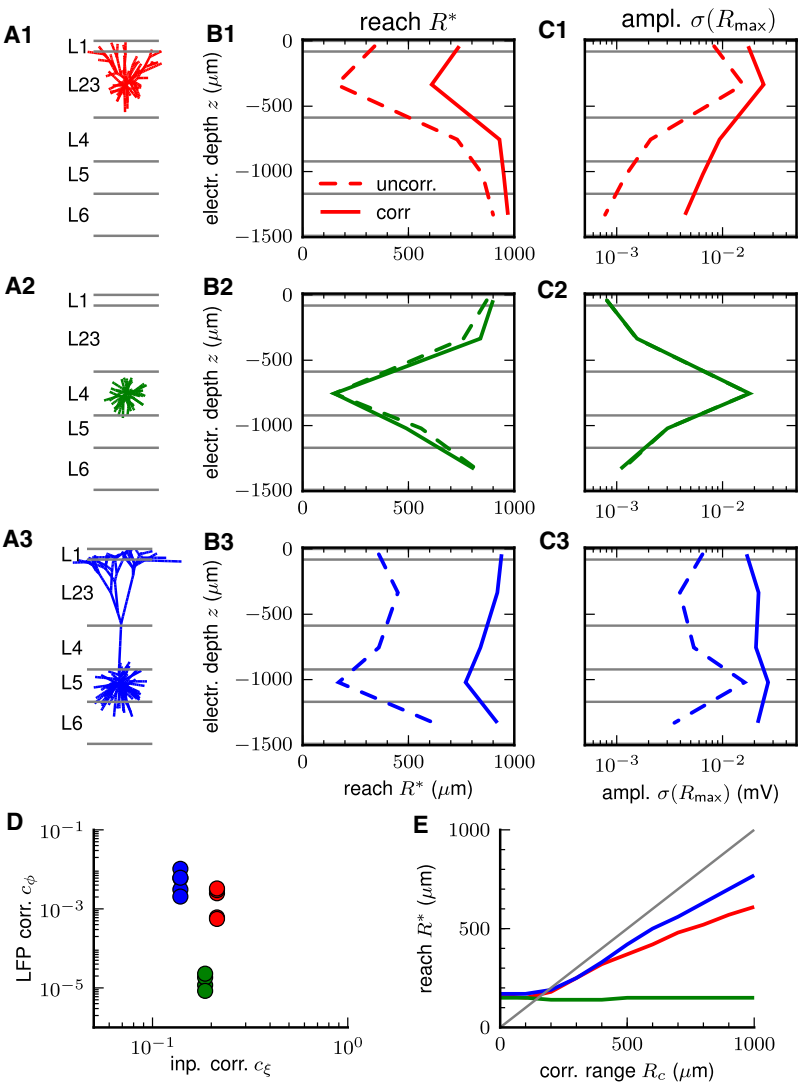

Figure 6. Input from Cortical-Network Model

LFP from population simulations where input spike trains were generated by a laminar cortical network model of integrate-and-fire neurons.

(A) Cell types of populations of L3 (A1), L4 (A2), and L5 (A3) cells.

(B and C) Reach R^* and amplitude $\sigma(R_{max} = 1{,}000\ \mu m)$ of LFP as a function of electrode depth z for the LFP generated individually by the three neuronal populations.

(D) Resulting correlation between single-cell LFP contributions c_ϕ and input correlations c_ξ for the three different neuronal populations (indicated by color). Different dots represent recording positions in the different cortical layers.

(E) LFP reach computed in the soma layer for different spatial ranges of input correlation R_c (as in Figure 5) for the three different cell populations (indicated by color).

2009; Sakata and Harris, 2009); corresponding data from cat cortex is to our knowledge not available). In addition, we generated uncorrelated Poissonian spike trains representing background activity from distant cortical areas. The populations of morphologically reconstructed neurons received a selection of input spike trains from the laminar network and background activity based on the morphology and connectivity of each cell type. In this way each cell in the populations of reconstructed cells had on average the same number of incoming synapses as a cell in the laminar network resulting in the same mean synaptic input (see Supplemental Information). Synapses were distributed differently across the dendritic tree of the reconstructed cells depending on the origin of the presynaptic cell type (see Supplemental Information). This setup produced input correlations c_ξ and correlations between single cell LFP contributions c_ϕ, that were specific for each population.

The resulting input correlations c_ξ between total input currents and LFP correlation c_ϕ are comparable to our previous simulations (Figure 6D, compare with Figure 4G). The L5 population produced larger LFP correlations c_ϕ than the L3 and L4 populations even though the input correlation c_ξ was lower, in line with the above results (Figure 4G). We computed the LFP amplitude for three different populations (of the same types as before, Figure 6B) for different cortical depths. Similar to the generic scenarios for the case of uncorrelated synaptic inputs (Figure 3), both the reach and amplitude vary with cortical depth with a minimum reach R^*, and maximum amplitude σ in the soma layer of each population. Further, the level of input correlations provided by the spontaneous spiking activity of the laminar cortical network was sufficient to increase both the reach and amplitude of the LFP for the L3 and L5 populations as compared to the situation where the LFP contributions from different cells would have been uncorrelated (Figures 6B and 6C, dashed lines; by setting $R_c = 0$; see Experimental Procedures and Equation 12). The reach of the LFP from the L4 population was similar to the situation with uncorrelated synaptic input.

In Figure 6B, we assumed that each neuron draws its inputs from the same (statistical) ensemble of presynaptic spike trains, resulting in the same input correlation in the whole population. We next calculated the LFP reach in the soma layer for the three different populations assuming that only LFP contributions from cells within a radius R_c were correlated and contributions from cells outside this region were uncorrelated (see Experimental Procedures and Equation 12). Also here we found that for the pyramidal cell populations the LFP reach was largely determined by the spatial scale of correlated activity while the LFP reach for the L4 population was largely unaffected by the spatial scale of correlations (Figure 6E).

DISCUSSION

We have investigated a biophysically detailed model of LFP generation and provided an intuitive simplified model to interpret

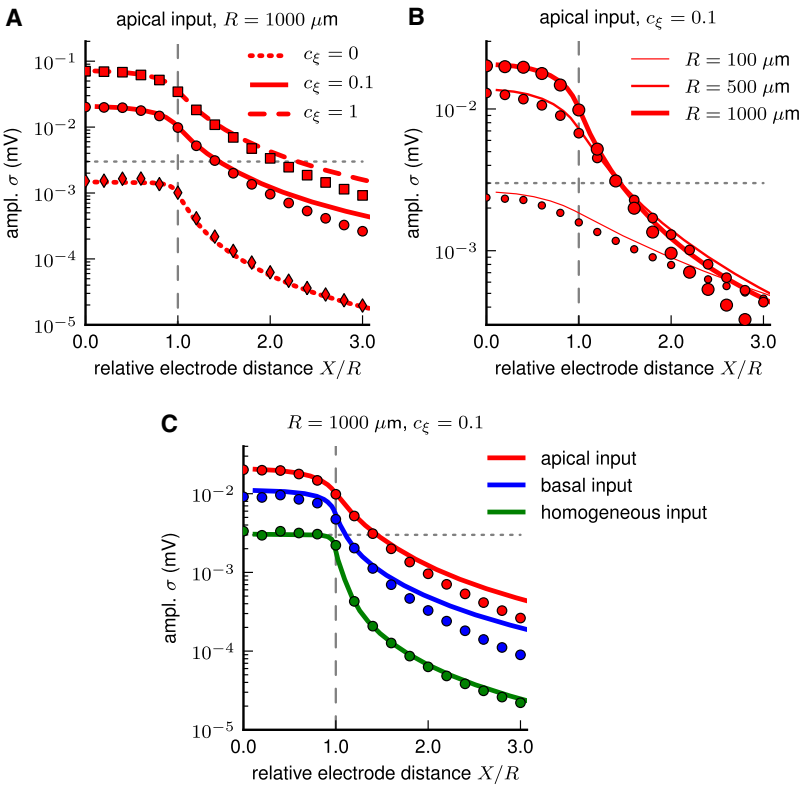

Figure 7. Amplitude of the LFP Generated by a Distant L5 Pyramidal Cell Population of Radius *R*

Dependence of the soma layer LFP amplitude σ on the relative horizontal distance X/R between the electrode and the population center for (A) different input correlations c_ξ (R = 1,000 μm, apical input), (B) different population sizes R (c_ξ = 0.1, apical input), and (C) different synaptic-input distributions (R = 1,000 μm, c_ξ = 0.1; see legends and panel titles). Curves and symbols correspond to results obtained from the simplified model (using numerically extracted shape functions $f(r)$; see Simplified Model of Population LFP Signals) and simulations of the full model (see LFP Simulations), respectively. Dashed vertical lines mark situation with electrode on population edge (X/R = 1). For comparison, horizontal dotted lines show soma layer LFP amplitude σ generated by a local population of L5 pyramidal cells receiving uncorrelated homogeneously distributed synaptic input (X = 0, R = 1,000 μm, c_ξ = 0; cf. solid curve in Figure 3E3).

our results. If the synaptic input to the neurons in the vicinity of a recording electrode always had been uncorrelated, we could have reported the following simple rule of thumb: almost all of the LFP signal measured by an electrode comes from neurons within a lateral distance of about 200 μm. This estimate is in accordance with recent results by Katzner et al. (2009) and Xing et al. (2009). The independence of the *spatial reach*, i.e., the size of the region generating the LFP, from the morphology of the neurons in the population and the spatial distribution of the synapses may be at odds with common thinking on the origin of the LFP emphasizing the distinction between open-field (pyramidal) and closed-field (stellate) neurons (Lorente de No, 1947; Johnston and Wu, 1995), and this highlights the importance of a thorough quantitative investigation of the origin of LFP.

The situation when the synaptic input to the neuronal population is correlated is, however, more in line with common thinking regarding the dominant contributions from pyramidal neurons, but only when the input is spatially asymmetric, i.e., solely onto either the basal or apical dendritic branches. In this case correlated synaptic inputs were found to give correlated neuronal LFP sources and consequently an amplified LFP signal. With homogeneous inputs onto pyramidal neurons, this correlation transfer is observed to be very weak, resulting in very little such correlation amplification. For the stellate layer 4 neurons with very symmetric dendritic branching, the LFP contributions from individual neurons were found to be essentially uncorrelated, independent of the level of synaptic input correlations. With spike-train correlations present in the synaptic input, as in our laminar network example in Figure 6, one might thus expect pyramidal neurons to give larger LFP contributions than the stellate neurons. Given the observed strong dependence on input correlations and spatial distribution of the synaptic inputs, our model study thus suggests several possible explanations for the significant variation for the reach of the LFP seen in various experimental studies (Kreiman et al., 2006; Liu and Newsome, 2006; Berens et al., 2008a; Katzner et al., 2009; Xing et al., 2009). As the level of synaptic input correlations depends on the state of cortical network, it follows that the LFP reach in general will not be a static fixed quantity, even for a particular fixed electrode in a particular experiment.

We also find the population LFP to depend strongly on the depth position of the recording electrode. With the electrode placed above or below the dendrites of the generating population, as, e.g., for recordings done in L4, L5 or L6 with an active L3 population depicted in Figure 3, the reach is much larger than for recordings done in the soma layer (L2/3). However, the LFP amplitudes recorded in these lower layers are tiny in comparison. With the electrode placed in a layer with substantial synaptic inputs onto neurons with their somata located in a different cortical layer (e.g., recordings in L2/3 with a L5 population receiving apical synaptic input), the reach and the amplitude are comparable to what is recorded in the soma layer of the active population. Thus, in an experimental setting, it seems natural to conjecture that the LFP recorded by an electrode is dominated by populations with substantial synaptic processes in the recording layer. Sizable contributions from populations with neurons positioned entirely above or below the electrode cannot be ruled out, however.

In our study, we took on an "electrode-centric" view, i.e., we used the size of the region of LFP generators as a measure of the spatial reach. An alternative "population-centric" view would be to focus on the effective LFP signal spread from a population and to ask how far outside an active population the LFP signal extends. Our approach can be easily extended to study this alternative measure of LFP locality. Figure 7 shows results for

the LFP amplitude in the soma layer of a population of layer 5 neurons when the recording electrode is placed at different positions X away from the center of the population. Figure 7A showing results for apical synaptic input for a population radius of 1 mm highlights the dominant role of synaptic-input correlations for the case of asymmetric input: not only is the LFP amplitude highly amplified compared to the uncorrelated case, the LFP signal also extends much further outside the population. For example, in the fully correlated case ($c_\xi = 1$), the LFP amplitude measured 2 mm outside the population ($X/R = 3$) is similar to the LFP measured in the center of the population with uncorrelated input ($c_\xi = 0$). Figure 7B shows that the decay in relative terms, i.e., with electrode position X measured in units of the population radius R, is less sharp for the smaller populations, simply reflecting that the spatial blurring inherent in the generation of LFP will be more pronounced in this case. Figure 7C further demonstrates the crucial role played by the spatial distribution of synaptic inputs in amplifying the LFP signal in the case of correlated input. For this example with $c_\xi = 0.1$, the resulting LFP is much larger both for apical and basal inputs than for homogeneous inputs. For the homogeneous-input case, we in fact observe very little effect of the correlations in the synaptic input as the LFP amplitude inside the population is almost the same as at the center of the same population in the case of uncorrelated input (dotted horizontal line in the panels). The simplified model (lines in Figure 7) generally accounts well for the observed simulation results (symbols in Figure 7) also for the off-center electrode, except for a systematic deviation at the largest electrode distances for apical and basal input: Here, the simulation results decay faster than predicted by the simplified model. While this point may have little relevance for the practical interpretation of LFP signals, it reflects an interesting physical point: when moving horizontally away from a population of pyramidal neurons receiving correlated asymmetric input so that a sizable vertical current dipole is set up, the decay will go as $1/X^3$ rather than $1/X^2$ as predicted by the present version of the simplified model (Pettersen and Einevoll, 2008). If warranted, our present simplified model could be extended to account for this by, e.g., incorporating shape functions f that depend explicitly on correlations, spatial distributions of synaptic inputs and/or direction.

Simultaneously recorded LFP signals at different sites have been found to be highly correlated up to several millimeters apart with a spatial fall-off that depends on the cortical state (Destexhe et al., 1999; Nauhaus et al., 2009). How should such cross-correlations between LFP signals recorded by two electrodes positioned, say, one millimeter apart, be interpreted? Our results rule out that the two LFP signals are generated by uncorrelated synaptic activity and that the activity around one electrode spreads by volume conduction to the other. This would require the electrodes to be less than half a millimeter apart. A more likely reason for the observed cross-correlations is that the neurons located around the two separate electrodes receive correlated synaptic input. As seen in Figure 7, however, the signal LFP from populations receiving asymmetric correlated synaptic inputs may be very strong and extend far outside the population itself. It therefore cannot be ruled out that the synaptic input in the vicinity of the electrodes is uncorrelated, and that both electrodes pick up LFP signals from such a distant correlated population.

The neuronal connectivity will affect the LFP in two ways: first by determining the spike-train statistics in the network and second by determining how the resulting spike-train statistics, in our case the spike-train correlations are ''translated'' into correlations between the neuronal LFP contributions setting up the population LFP. Our study has focused solely on the latter effect as these synaptic input correlations have been imposed on our models. This makes our result more applicable since our results then more easily can be adapted to future research projects with various types of spiking neural networks: calculated input correlations in new network models can be combined with the results presented here to give model LFP predictions.

Here, we have not studied different frequency components of the LFP separately. Instead, by focusing on the amplitude of the LFP, i.e., the (square root of the) integral of the LFP power spectrum (Wiener-Khinchin theorem; see e.g., Papoulis and Pillai, 2002), we have used a frequency-independent measure of the LFP reach. Due to the intrinsic dendritic filtering of the LFP contributions from individual neurons (Pettersen and Einevoll, 2008; Lindén et al., 2010), the spatial LFP reach will, however, likely depend on frequency. Additional effects can arise if the electrical conductivity of the extracellular medium itself is frequency dependent (Bédard et al., 2004), but such a frequency dependence has been challenged by a recent experimental study of tissue in monkey motor cortex (Logothetis et al., 2007). Our modeling approach can in any case be generalized to investigate each frequency component separately. Such a study will be important for the interpretation of experimental results of stimulus-evoked LFP which has indicated frequency dependence both in the tuning properties (Liu and Newsome, 2006; Berens et al., 2008b) and in the information content (Belitski et al., 2008) of the LFP. However, the LFP amplitude of each frequency component will also be proportional to the amplitude of the corresponding frequency component of the presynaptic spike trains, and this will naturally vary with the spiking dynamics of the network in question.

Our analysis has focused on LFP recorded in a unipolar fashion with a ground reference positioned far away. The formalism can equally well be used to model bipolar, i.e., differential, LFP since it is straightforwardly found by subtraction of unipolar LFPs. Likewise, the formalism has already been used to probe the neural origin of the current-source density (CSD) and test various candidate methods for estimating CSD using model-based LFP data for which the ground-truth CSD is known (Pettersen et al., 2006; Łęski et al., 2011). Another application of the present approach would be to address the question of the neural origin of the electrical potentials recorded outside the brain, that is, the EEG signal. The present biophysical forward-modeling formalism is, with some modifications to account for the electrical dampening by the scull and scalp (Nunez, 2006), well suited also to address this question. The large distance between the EEG electrodes and neural sources implies that the signal will get contributions from a larger collection of neural populations than the LFP, and the underlying convoluted cortical surface will also introduce additional geometrical issues which must be taken into account. While we do not address this

question here, we can already see from Figure 3 why the spatial reach of the EEG will be larger than for the LFP. For the layer-1 electrode positioned close to the cortical surface, the reach is seen in Figures 3D1–3D3 to be much larger than in the soma layer. For the EEG electrodes this effect will expectedly be further enhanced making the predicted spatial reach of EEG even larger. The results in Figure 3 are for uncorrelated sources, however, and the formation of the EEG signal will also depend on the level of correlations in the various contributing populations.

In the present study, we have focused on neurons with passive dendrites and current-based synaptic inputs, making our models fully linear. This simplification allowed for the identification of three key factors determining the population LFP, i.e., the single-neuron LFP shape function and the correlation between, and density of, neuronal LFP sources. Likewise, our results only address the LFP set up by well-organized laminar neuronal populations as seen, for example, in cortex and hippocampus and do not necessarily apply to subcortical structures with other neuron types and geometrical arrangements. However, active dendritic conductances and other geometrical arrangements can straightforwardly be included into the simulation formalism, and we believe this type of biophysically detailed modeling will become an unavoidable tool in the quantitative interpretation of the type of data that can be recorded with the new generation of silicon-based multielectrodes (Buzsáki, 2004).

EXPERIMENTAL PROCEDURES

Here, we outline the main features of a simplified model which allows us to gain intuitive understanding of the LFP reach (Simplified Model of Population LFP Signals), and describe the detailed models and procedures used in the simulations of neurons with realistic morphologies (LFP Simulations).

Simplified Model of Population LFP Signals

Outline of Derivation

A comprehensive derivation can be found in Supplemental Procedures, and a table over the notation can be found in Table S1.

We consider a population of neurons where a synaptic input current $\xi_{ij}(t)$ at synapse j onto neuron i causes a transmembrane current density $i_{ij}^m(t,\vec{r})$ which, in turn, gives rise to the following extracellular electrical potential $\phi_{ij}(t)$ measured by an electrode at position $\vec{r}=0$ (Holt and Koch, 1999; Lindén et al., 2010):

$$\phi_{ij}(t)=\frac{1}{4\pi\sigma_{cond}}\int_{-\infty}^{\infty}d\vec{r}\,\frac{i_{ij}^m(t,\vec{r})}{|\vec{r}|}. \tag{3}$$

Here σ_{cond} is the scalar and homogeneous electrical conductivity.

Under our assumption of linear synapses and dendrites, and ignoring intrinsic dendritic filtering effects (Lindén et al., 2010), the LFP contribution decomposes into a time-dependent part $\xi_{ij}(t)$ and a shape factor f_{ij},

$$\phi_{ij}(t)=f_{ij}\xi_{ij}(t). \tag{4}$$

With the further assumption that the synaptic inputs $\xi_{ij}(t)$ onto neuron i are statistically independent of the shape factors f_{ij}, one can approximate the LFP generated by neuron i as

$$\phi_i(t)=\xi_i(t)f(r_i), \tag{5}$$

where $\xi_i(t)$ is the total synaptic input, and $f(r_i)$ is the single-neuron shape function of the type illustrated in Figure 2.

The variance of the compound LFP signal in the center of a population of radius R is then, after some algebra, found to be

$$\sigma^2(R)=E_t\left[\phi(t)^2\right]=\sigma_\xi^2((1-c_\xi)g_0(R)+c_\xi g_1(R)) \tag{6}$$

where

$$g_0(R)\equiv 2\pi\rho\int_0^R dr\,r\,f(r)^2 \text{ and } g_1(R)\equiv 4\pi^2\rho^2\left(\int_0^R dr\,r\,f(r)\right)^2. \tag{7}$$

For convenience, we now, without loss of generality, set $\sigma_\xi^2=1$.

To illustrate how the shape of $f(r)$ determines the (existence of a) reach of a population signal we consider a power-law shape function

$$f(r)=\begin{cases}1 & r<\epsilon\\ \epsilon^\gamma r^{-\gamma} & r\geq\epsilon\end{cases} \tag{8}$$

with a decay exponent $\gamma\geq 0$ and a cutoff distance ϵ. Introducing the cutoff distance ϵ is necessary to avoid a singularity at $r=0$. With Equation 8, the functions $g_0(R)$ and $g_1(R)$ in Equation 7 read

$$g_0(R)=\begin{cases}2\pi\rho\left[\frac{1}{2}\epsilon^2+\epsilon^{2\gamma}\ln\frac{R}{\epsilon}\right] & \gamma=1\\ 2\pi\rho\left[\frac{1}{2}\epsilon^2+\frac{\epsilon^{2\gamma}}{2-2\gamma}\left(R^{2-2\gamma}-\epsilon^{2-2\gamma}\right)\right] & \gamma\neq 1\end{cases}$$
$$g_1(R)=\begin{cases}4\pi^2\rho^2\left[\frac{1}{2}\epsilon^2+\epsilon^{\gamma}\ln\frac{R}{\epsilon}\right]^2 & \gamma=2\\ 4\pi^2\rho^2\left[\frac{1}{2}\epsilon^2+\frac{\epsilon^{\gamma}}{2-\gamma}\left(R^{2-\gamma}-\epsilon^{2-\gamma}\right)\right]^2 & \gamma\neq 2\end{cases} \tag{9}$$

Consider first the case $c_\xi=0$ (uncorrelated input): if $\gamma>1$, $g_0(R)$ converges with increasing population size R to a constant value, and the amplitude $\sigma(R)$ of the compound signal thus saturates. For a population of dipoles in the far-field limit ($\gamma=2$), the spatial reach can therefore be defined. For $\gamma<1$, however, $g_0(R)$ and, in turn, the compound amplitude $\sigma(R)$ diverge as R approaches infinity. In this case, a finite spatial reach does not exist according to our definition of the term. If the input is correlated ($c_\xi>0$), the second term in Equation 6 converges only for $\gamma>2$. Here, even the LFP from a population of dipoles diverges with increasing population size. Note that for large neuron densities ρ, the second term in Equation 6 will dominate even for small correlations c_ξ; see Figure S1.

The calculations for the case with off-center electrodes shown in Figure 7 proceed in an analogous way. The only difference is that the lack of circular symmetry prevents the simplification into the one-dimensional integral formulation in Equation 6, and two-dimensional integrals must be performed instead.

Comparison with Simulation Results

The simplified model presented here illustrates that the amplitude of the extracellular compound potential of a population of neurons is essentially determined by the distance dependence $f(r)$ of the single-cell potentials, the density ρ, and the statistics of the synaptic input given by σ_ξ^2 and c_ξ. For simplified cell morphologies (e.g., current dipoles), the shape function $f(r)$ can be calculated analytically. In the present study, however, we investigate the compound signal of a population of neurons with realistic morphologies. To compare the predictions of the simplified model with simulation results, we therefore numerically evaluate the shape functions $f(r)$ for different morphologies, synapse distributions, and electrode depths in single-neuron simulations (see Results; Figure 2) and compute the corresponding functions $g_0(R)$ and $g_1(R)$ according to Equation 7. For known input statistics σ_ξ and c_ξ, we can, by means of (6), predict the compound amplitude $\sigma(R)$ for different population sizes R.

As a consequence of our assumption of no synapse-specific temporal filtering, the synaptic input current $\xi_i(t)$ is proportional to the single-cell potential $\phi_i(t)$. The correlation coefficient c_ξ is therefore identical to the correlation $c_\phi=E_t[\phi_i(t)\phi_j(t)]/\sqrt{E_t[\phi_i^2(t)]E_t[\phi_j^2(t)]}$ of the potentials $\phi_i(t)$. This would not hold if the synapse-specific filtering of the input currents was taken into account (see Tetzlaff et al., 2008), and we will therefore regard the "input" $\xi_i(t)$ as the time-dependent part of the single-source potential $\phi_i(t)$ rather than as the total synaptic input current, and replace the correlation coefficient c_ξ in Equation 6 by the correlation c_ϕ between single-cell potentials, i.e.,

$$\sigma(R)=\sqrt{(1-c_\phi)g_0(R)+c_\phi g_1(R)}. \tag{10}$$

corresponding to Equation 1. The transfer of correlations $c_\xi \to c_\phi$ from input currents to potentials is, in a realistic setting (i.e., for frequency dependent current-density filters), nontrivial. A rigorous mathematical treatment of this is beyond the scope of this work. Instead, we investigate the current-potential correlation transfer for different neuron types and synapse distributions numerically (see Results; Figure 4).

LFP Simulations

Below follows a summary of the numerical simulations based on reconstructed morphologies. For tables containing model details and parameter values, see Tables S2–S4.

Population Geometry

Multicompartment neuron models with morphologies from digital cell reconstructions (see below) were randomly positioned in a cylindrical volume with radius 1,000 μm. Each population consisted of 10,000 cells with identical cell morphology but each cell was randomly rotated along the z axis. The somata of all cells in a population were placed at the same cortical depth, chosen as the midpoint of the corresponding cortical layer. Layer boundaries were derived from Stepanyants et al. (2008). The same x and y coordinates were used for populations of the three different cell types to remove variability due to the exact cell positioning when comparing different cell types. See Supplemental Experimental Procedures for details.

Neuron Models and Simulations

We used morphological reconstructions of L3 pyramidal, L4 spiny stellate, and L5 pyramidal neurons (Mainen and Sejnowski, 1996) downloaded from ModelDB (http://senselab.med.yale.edu/modeldb) from which we removed axon compartments and active conductances (making the models passive). For passive parameters and details on spatial segmentation, see Supplemental Experimental Procedures.

Simulations were performed with a time resolution of 0.0625 ms and resulting data was stored with a time resolution of 1.0 ms. Simulations were in all applications run for a time period of 1200 ms were the first 200 ms were removed before analysis to avoid any upstart effects in the simulations.

Synapse Models, Placement, and Input

Postsynaptic currents (PSCs) were modeled as α-currents triggered by the arrival of presynaptic input spikes (for details, see Supplemental Experimental Procedures). For the results shown in Figures 2, 3, 4, 5, and 7, only excitatory synapses (EPSCs) were used, while both excitatory and inhibitory synapses (IPSCs) were used in the simulations with laminar-network input (Figure 6; see below). The amplitude of a single IPSC was four times stronger than an EPSC. Note: since the neuron models are linear with respect to the amplitude of current injection, the results will not change with other values of the input current (as long as the relative values for excitatory and inhibitory synapses are fixed) except a rescaling of the resulting LFP amplitudes.

Synapses were randomly assigned to compartments within certain cortical depths determined by the type of synaptic activation (apical/homogeneous/basal) and cell type (see Figure 2A). These depths were determined by the soma positions and layer boundaries, as described in the Tables S2–S4. The probability for a synapse being placed on a specific compartment was proportional to the relative membrane area of that compartment compared to the total membrane area within the allowed cortical depths, resulting in homogeneous synapse densities with respect to the membrane area of the dendrites. No synapses were placed on the soma.

Distributions and number of synapses onto the dendrites of the neurons were different in simulations with uncorrelated input spike trains or spike trains using the common-input model (Figures 2, 3, 4, 5, and 7) than in the simulations for the laminar network model (Figure 6). See Supplemental Experimental Procedures for details.

We considered three different types of input spike-train ensembles: uncorrelated stationary Poisson input, correlated stationary Poisson input generated by a shared-input model, and input from a laminar-network model. Details and parameters are given in Tables S2–S7.

Calculation of LFP Amplitude and Reach

We computed the unipolar LFP, i.e., LFP recorded with reference to a ground electrode positioned far way, using the line-source method described by Holt and Koch (1999) (see also Holt, 1998, for method description). This involves summing over all transmembrane currents weighted inversely with the distance between the recording electrode and the compartments in the multi-compartment neuron model. The population LFP was computed by first calculating the contributions from single neurons separately and then summing over these contributions from all cells within the population. Cells were assumed to be surrounded by a purely resistive infinite extracellular medium with conductivity σ_{cond} = 0.3 S/m. No filtering was applied to the resulting LFP signal.

The amplitude σ of the LFP signal from a population was computed through the variance over time in the 1,000 ms simulation time interval:

$$\sigma^2(R) = \mathrm{E}_t\left[\left(\phi(t) - \mathrm{E}_t[\phi(t)]\right)^2\right] \quad (11)$$

where $\mathrm{E}_t[\cdot]$ denotes time average and $\phi = \sum_{\{i|r_i<R\}} \phi_i$ is the sum of LFP contributions ϕ_i from cells within population radius R. In situations where the LFP contributions were assumed to be correlated only within a region $R_c<R$ (Figures 5 and 6), the amplitude $\sigma(R)$ was computed from

$$\sigma^2(R) = \mathrm{E}_t\left[\left(\phi_{R_c}(t) - \mathrm{E}_t\left[\phi_{R_c}(t)\right]\right)^2\right] + \sum_{\{i|R_c<r_i<R\}} \mathrm{E}_t\left[\left(\phi_i(t) - \mathrm{E}_t[\phi_i(t)]\right)^2\right] \quad (12)$$

where $\phi_{R_c} = \sum_{\{i|r_i<R_c\}} \phi_i$ is the summed LFP signal from cells within radius R_c. For the results in Figure 6, R_c was set to 0 for the "uncorrelated" networks.

The spatial reach of the LFP was defined as

$$R^* \equiv \min(\{R | \sigma(R)/\sigma(R_{\max}) = 0.95\}) \quad (13)$$

with $R_{\max}$ = 1 mm.

Measurement of Synaptic-Current and LFP Correlations

We characterize the level of correlations between total synaptic input currents $\xi_i(t)$ or single-cell LFPs $\phi_i(t)$ by the population averaged pairwise correlation coefficient $c_x = \mathrm{E}_{i,j\neq i}[c_x^{ij}]$ with $c_x^{ij} = \mathrm{Cov}_t[x_i(t), x_j(t)]/\sqrt{\mathrm{Var}_t[x_i(t)]\mathrm{Var}_t[x_j(t)]}$. Here, $x_i(t)$ is used as a placeholder for either $\xi_i(t)$ or $\phi_i(t)$. The variances $\mathrm{Var}_t[x_i(t)] = \mathrm{E}_t[x_i(t)^2] - \mathrm{E}_t[x_i(t)]^2$ and covariances $\mathrm{Cov}_t[x_i(t), x_j(t)] = \mathrm{E}_t[x_i(t)x_j(t)] - \mathrm{E}_t[x_i(t)]\mathrm{E}_t[x_j(t)]$ are defined as time averages (indicated by the subscript t). For a homogeneous ensemble of signals $x_i(t)$ $(i = 1, \ldots, N)$ with identical variances $\sigma_x^2 = \mathrm{Var}_t[x_i(t)]$ $(\forall i)$, the population averaged correlation coefficient c_x can be obtained from the variance

$$\mathrm{Var}_t[z(t)] = \sum_{i=1}^{N} \mathrm{Var}_t[x_i(t)] + \sum_{i=1}^{N}\sum_{j\neq i}^{N} \mathrm{Cov}_t[x_i(t), x_j(t)] = \sigma_x^2(N + N[N-1]c_x) \quad (14)$$

of the compound signal $z(t) = \sum_{i=1}^{N} x_i(t)$ and the variance σ_x^2 of the individual signals. In the context of this study, however, the ensemble of signals is not homogeneous: the variance $\mathrm{Var}_t[x_i(t)]$ of the single-cell LFP $x_i(t) = \phi_i(t)$ systematically depends on the distance of the neuron i from the electrode tip (see LFP Simulations). We therefore first standardize (homogenize) the individual signals, $\tilde{x}_i(t) = (x_i(t) - \mathrm{E}_t[x_i(t)])/\sqrt{\mathrm{Var}_t[x_i(t)]}$, such that $\mathrm{Var}_t[\tilde{x}_i(t)] = 1$ $(\forall i)$. Note that this standardization does not change the pairwise correlation coefficients c_x^{ij} as defined above. From the variance $\mathrm{Var}_t[\tilde{z}(t)] = N + N(N-1)c_x$ of the resulting compound signal $\tilde{z}(t) = \sum_{i=1}^{N} \tilde{x}_i(t)$ we obtain the population averaged correlation coefficient

$$c_x = \frac{\mathrm{Var}_t\left[\tilde{z}(t)\right] - N}{N(N-1)}. \quad (15)$$

Software

Simulations with reconstructed cells were performed with NEURON (Carnevale and Hines, 2006; http://www.neuron.yale.edu) using the supplied Python interface (Hines et al., 2009). The laminar network of integrate-and-fire neurons was simulated using NEST (Gewaltig and Diesmann, 2007; http://www.nest-initiative.org). Data analysis and plotting was done in Python (http://www.python.org) using the IPython, Numpy, Scipy, Matplotlib, and NeuroTools packages.

SUPPLEMENTAL INFORMATION

Supplemental Information includes one figure, seven tables, and Supplemental Experimental Procedures and can be found with this article online at doi:10.1016/j.neuron.2011.11.006.

ACKNOWLEDGMENTS

We thank the anonymous reviewers for their very useful suggestions. This work was partially funded by the Research Council of Norway (eVita [eNEURO], NOTUR), EU Grant 15879 (FACETS), EU Grant 269921 (BrainScaleS), BMBF Grant 01GQ0420 to BCCN Freiburg, Next-Generation Supercomputer Project of MEXT, Japan, and the Helmholtz Alliance on Systems Biology.

Accepted: November 18, 2011
Published: December 7, 2011

REFERENCES

Andersen, R.A., Musallam, S., and Pesaran, B. (2004). Selecting the signals for a brain-machine interface. Curr. Opin. Neurobiol. *14*, 720–726.

Bédard, C., Kröger, H., and Destexhe, A. (2004). Modeling extracellular field potentials and the frequency-filtering properties of extracellular space. Biophys. J. *86*, 1829–1842.

Belitski, A., Gretton, A., Magri, C., Murayama, Y., Montemurro, M.A., Logothetis, N.K., and Panzeri, S. (2008). Low-frequency local field potentials and spikes in primary visual cortex convey independent visual information. J. Neurosci. *28*, 5696–5709.

Berens, P., Keliris, G.A., Ecker, A.S., Logothetis, N.K., and Tolias, A.S. (2008a). Comparing the feature selectivity of the gamma-band of the local field potential and the underlying spiking activity in primate visual cortex. Front. Syst. Neurosci. *2*, 2.

Berens, P., Keliris, G.A., Ecker, A.S., Logothetis, N.K., and Tolias, A.S. (2008b). Feature selectivity of the gamma-band of the local field potential in primate primary visual cortex. Front. Neurosci. *2*, 199–207.

Binzegger, T., Douglas, R.J., and Martin, K.A. (2004). A quantitative map of the circuit of cat primary visual cortex. J. Neurosci. *24*, 8441–8453.

Braitenberg, V., and Schüz, A. (1998). Cortex: Statistics and Geometry of Neuronal Connectivity (Berlin: Springer).

Buzsáki, G. (2004). Large-scale recording of neuronal ensembles. Nat. Neurosci. *7*, 446–451.

Carnevale, N.T., and Hines, M.L. (2006). The NEURON Book (Cambridge: Cambridge University Press).

Colgin, L.L., Denninger, T., Fyhn, M., Hafting, T., Bonnevie, T., Jensen, O., Moser, M.-B., and Moser, E.I. (2009). Frequency of gamma oscillations routes flow of information in the hippocampus. Nature *462*, 353–357.

de Kock, C.P.J., and Sakmann, B. (2009). Spiking in primary somatosensory cortex during natural whisking in awake head-restrained rats is cell-type specific. Proc. Natl. Acad. Sci. USA *106*, 16446–16450.

Denker, M., Riehle, A., Diesmann, M., and Grün, S. (2010). Estimating the contribution of assembly activity to cortical dynamics from spike and population measures. J. Comput. Neurosci. *29*, 599–613.

Denker, M., Roux, S., Lindén, H., Diesmann, M., Riehle, A., and Grün, S. (2011). The local field potential reflects surplus spike synchrony. Cereb. Cortex *21*, 2681–2695.

Destexhe, A., Contreras, D., and Steriade, M. (1999). Spatiotemporal analysis of local field potentials and unit discharges in cat cerebral cortex during natural wake and sleep states. J. Neurosci. *19*, 4595–4608.

Di, S., Baumgartner, C., and Barth, D.S. (1990). Laminar analysis of extracellular field potentials in rat vibrissa/barrel cortex. J. Neurophysiol. *63*, 832–840.

Einevoll, G.T., Pettersen, K.H., Devor, A., Ulbert, I., Halgren, E., and Dale, A.M. (2007). Laminar population analysis: estimating firing rates and evoked synaptic activity from multielectrode recordings in rat barrel cortex. J. Neurophysiol. *97*, 2174–2190.

Gewaltig, M.-O., and Diesmann, M. (2007). NEST (NEural Simulation Tool). Scholarpedia *2*, 1430.

Henrie, J.A., and Shapley, R. (2005). LFP power spectra in V1 cortex: the graded effect of stimulus contrast. J. Neurophysiol. *94*, 479–490.

Hines, M.L., Davison, A.P., and Muller, E. (2009). NEURON and Python. Front. Neuroinf. *3*, 1.

Holt, G.R. (1998). A Critical Reexamination of Some Assumptions and Implications of Cable Theory in Neurobiology (PhD thesis, California Institute of Technology, Pasadena, CA).

Holt, G.R., and Koch, C. (1999). Electrical interactions via the extracellular potential near cell bodies. J. Comput. Neurosci. *6*, 169–184.

Johnston, D., and Wu, S.M.-S. (1995). Foundations of Cellular Neurophysiology (Cambridge, MA: MIT Press).

Kandel, A., and Buzsáki, G. (1997). Cellular-synaptic generation of sleep spindles, spike-and-wave discharges, and evoked thalamocortical responses in the neocortex of the rat. J. Neurosci. *17*, 6783–6797.

Katzner, S., Nauhaus, I., Benucci, A., Bonin, V., Ringach, D.L., and Carandini, M. (2009). Local origin of field potentials in visual cortex. Neuron *61*, 35–41.

Kelly, R.C., Smith, M.A., Kass, R.E., and Lee, T.S. (2010). Local field potentials indicate network state and account for neuronal response variability. J. Comput. Neurosci. *29*, 567–579.

Kreiman, G., Hung, C.P., Kraskov, A., Quiroga, R.Q., Poggio, T., and DiCarlo, J.J. (2006). Object selectivity of local field potentials and spikes in the macaque inferior temporal cortex. Neuron *49*, 433–445.

Łęski, S., Pettersen, K.H., Tunstall, B., Einevoll, G.T., Gigg, J., and Wójcik, D.K. (2011). Inverse current source density method in two dimensions: inferring neural activation from multielectrode recordings. Neuroinformatics *9*, 401–425.

Lindén, H., Pettersen, K.H., and Einevoll, G.T. (2010). Intrinsic dendritic filtering gives low-pass power spectra of local field potentials. J. Comput. Neurosci. *29*, 423–444.

Liu, J., and Newsome, W.T. (2006). Local field potential in cortical area MT: stimulus tuning and behavioral correlations. J. Neurosci. *26*, 7779–7790.

Logothetis, N.K., Kayser, C., and Oeltermann, A. (2007). In vivo measurement of cortical impedance spectrum in monkeys: implications for signal propagation. Neuron *55*, 809–823.

Lorente de No, R. (1947). Action potential of the motoneurons of the hypoglossus nucleus. J. Cell. Physiol. *29*, 207–287.

Mainen, Z.F., and Sejnowski, T.J. (1996). Influence of dendritic structure on firing pattern in model neocortical neurons. Nature *382*, 363–366.

Mehring, C., Rickert, J., Vaadia, E., Cardosa de Oliveira, S., Aertsen, A., and Rotter, S. (2003). Inference of hand movements from local field potentials in monkey motor cortex. Nat. Neurosci. *6*, 1253–1254.

Mitzdorf, U. (1985). Current source-density method and application in cat cerebral cortex: investigation of evoked potentials and EEG phenomena. Physiol. Rev. *65*, 37–100.

Montemurro, M.A., Rasch, M.J., Murayama, Y., Logothetis, N.K., and Panzeri, S. (2008). Phase-of-firing coding of natural visual stimuli in primary visual cortex. Curr. Biol. *18*, 375–380.

Montgomery, S.M., and Buzsáki, G.M. (2007). Gamma oscillations dynamically couple hippocampal CA3 and CA1 regions during memory task performance. Proc. Natl. Acad. Sci. USA *104*, 14495–14500.

Nauhaus, I., Busse, L., Carandini, M., and Ringach, D.L. (2009). Stimulus contrast modulates functional connectivity in visual cortex. Nat. Neurosci. *12*, 70–76.

Nunez, P.L. (2006). Electric Fields of the Brain: The Neurophysics of EEG (Oxford: Oxford University Press).

Papoulis, A., and Pillai, S.U. (2002). Probability, Random Variables, and Stochastic Processes (Boston: McGraw-Hill).

Pesaran, B., Pezaris, J.S., Sahani, M., Mitra, P.P., and Andersen, R.A. (2002). Temporal structure in neuronal activity during working memory in macaque parietal cortex. Nat. Neurosci. *5*, 805–811.

Pettersen, K.H., and Einevoll, G.T. (2008). Amplitude variability and extracellular low-pass filtering of neuronal spikes. Biophys. J. *94*, 784–802.

Pettersen, K.H., Devor, A., Ulbert, I., Dale, A.M., and Einevoll, G.T. (2006). Current-source density estimation based on inversion of electrostatic forward

solution: effects of finite extent of neuronal activity and conductivity discontinuities. J. Neurosci. Methods *154*, 116–133.

Pettersen, K.H., Hagen, E., and Einevoll, G.T. (2008). Estimation of population firing rates and current source densities from laminar electrode recordings. J. Comput. Neurosci. *24*, 291–313.

Potjans, T.C., and Diesmann, M. (2011). The cell-type specific connectivity of the local cortical network explains prominent features of neuronal activity. arXiv. (http://arxiv.org/abs/1106.5678v1)

Rall, W. (1962). Electrophysiology of a dendritic neuron model. Biophys. J. *2*, 145–167.

Rickert, J., Oliveira, S.C., Vaadia, E., Aertsen, A., Rotter, S., and Mehring, C. (2005). Encoding of movement direction in different frequency ranges of motor cortical local field potentials. J. Neurosci. *25*, 8815–8824.

Roux, S., Mackay, W.A., and Riehle, A. (2006). The pre-movement component of motor cortical local field potentials reflects the level of expectancy. Behav. Brain Res. *169*, 335–351.

Sakata, S., and Harris, K.D. (2009). Laminar structure of spontaneous and sensory-evoked population activity in auditory cortex. Neuron *64*, 404–418.

Scherberger, H., Jarvis, M.R., and Andersen, R.A. (2005). Cortical local field potential encodes movement intentions in the posterior parietal cortex. Neuron *46*, 347–354.

Schroeder, C.E., Mehta, A.D., and Givre, S.J. (1998). A spatiotemporal profile of visual system activation revealed by current source density analysis in the awake macaque. Cereb. Cortex *8*, 575–592.

Stepanyants, A., Hirsch, J.A., Martinez, L.M., Kisvárday, Z.F., Ferecskó, A.S., and Chklovskii, D.B. (2008). Local potential connectivity in cat primary visual cortex. Cereb. Cortex *18*, 13–28.

Szymanski, F.D., Garcia-Lazaro, J.A., and Schnupp, J.W. (2009). Current source density profiles of stimulus-specific adaptation in rat auditory cortex. J. Neurophysiol. *102*, 1483–1490.

Tetzlaff, T., Rotter, S., Stark, E., Abeles, M., Aertsen, A., and Diesmann, M. (2008). Dependence of neuronal correlations on filter characteristics and marginal spike train statistics. Neural Comput. *20*, 2133–2184.

Wagatsuma, N., Potjans, T.C., Diesmann, M., and Fukai, T. (2011). Layer-dependent attentional processing by top-down signals in a visual cortical microcircuit model. Front. Comput. Neurosci. *5*, 31.

Womelsdorf, T., Fries, P., Mitra, P.P., and Desimone, R. (2006). Gamma-band synchronization in visual cortex predicts speed of change detection. Nature *439*, 733–736.

Xing, D., Yeh, C.-I., and Shapley, R.M. (2009). Spatial spread of the local field potential and its laminar variation in visual cortex. J. Neurosci. *29*, 11540–11549.